Converting the nanodomains of a diblock-copolymer thin film from spheres to cylinders with an external electric field

M. W. Matsen[a)]
Department of Physics, University of Reading, Whiteknights, Reading RG6 6AF, United Kingdom

(Received 17 November 2005; accepted 30 December 2005; published online 21 February 2006)

We investigate the ability of an applied electric field to convert the morphology of a diblock-copolymer thin film from a monolayer of spherical domains embedded in the matrix to cylindrical domains that penetrate through the matrix. As expected, the applied field increases the relative stability of cylindrical domains, while simultaneously reducing the energy barrier that impedes the transition to cylinders. The effectiveness of the field is enhanced by a large dielectric contrast between the two block-copolymer components, particularly when the low-dielectric contrast component forms the matrix. Furthermore, the energy barrier is minimized by selecting sphere-forming diblock copolymers that are as compositionally symmetric as possible. Our calculations, which are the most quantitatively reliable to date, are performed using a numerically precise spectral algorithm based on self-consistent-field theory supplemented with an exact treatment for linear dielectric materials. © *2006 American Institute of Physics*.
[DOI: 10.1063/1.2170082]

I. INTRODUCTION

The natural tendency of block-copolymer materials to self-assemble into periodically ordered morphologies provides an efficient means of fabricating nanoscale structures.[1] An application currently under development involves the construction of ultrahigh-capacity data-storage devices, consisting of a dense array of magnetic columns each capable of storing a single bit.[2] One proposed idea is to coat a substrate with a thin film of diblock copolymer that self-assembles into a monolayer of hexagonally packed spherical micelles. The block-copolymer pattern is then transferred to the substrate by a chemical etching process that consumes the micelle cores at a much greater rate than the matrix.[3] In this way, the etching eventually exposes the substrate beneath each core while still masking the intervening area. With continued etching, small holes are drilled into the substrate and later filled with magnetic material. The ability of the magnetic columns to sustain a permanent dipole moment relies on a sufficient aspect ratio, but achieving it can be a problem because the depth of the holes is limited by the duration over which the block-copolymer mask is able to survive the etching process. Superior masks could be created if the block-copolymer minority domain formed perpendicular cylinders that traversed the entire film. This way, the removal of the minority domains could be accomplished without any significant damage to the majority component. Another application that would benefit from perpendicular cylindrical domains is the construction of nanoporous membranes.[4] In this case, the matrix could be cross-linked to give the film mechanical strength allowing the minority component to be chemically removed. The result would be a thin rubbery film with a dense array of pores through which nanosized particles could pass. In this case, it is crucial that the minority domains span the entire thickness of the film.

There is no difficulty in creating block-copolymer films with cylindrical domains; it is just a matter of selecting molecules of appropriate composition. The challenge is to orient the domains vertical to the substrate, because surface interactions generally prefer the horizontal orientation. Even when the preferential surface affinity is eliminated by an appropriate coating,[5] the film tends to produce a poorly ordered morphology containing a mixture of both orientations. A simple strategy is to start with a monolayer of spherical domains for which there is no issue of orientation and for which high degrees of hexagonal order are readily achieved.[6] Next a strong perpendicular electric field can be applied that couples to the dielectric contrast between the domains,[7] caus-

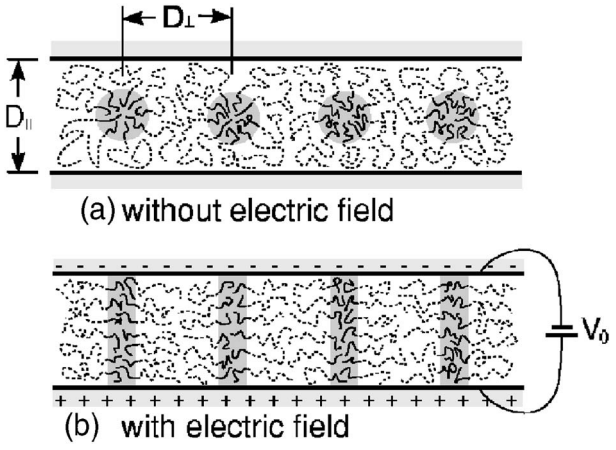

FIG. 1. (a) Monolayer of block-copolymer spherical micelles with a near-neighbor spacing of $D_\perp$ confined between two conducting plates separated by a distance of $D_\parallel$. (b) An applied voltage V_0 creates an external field of strength $E_0=V_0/D_\parallel$, transforming the spherical nanodomains into perpendicular cylinders.

[a)]Electronic mail: m.w.matsen@reading.ac.uk

ing the spheres to elongate in the direction of the field ultimately transforming into perpendicular cylinders as illustrated in Fig. 1.

Xu *et al.*[8] have already demonstrated that electric fields are able to transform spheres into perpendicular cylinders, although their experiments were performed on thicker films containing about ten layers. Their paper also presented some theoretical simulations to model the process, but not using equivalent parameters to those of the experiment. Although there is a general consensus that the electric-field mechanism involves the dielectric contrast, quantitative estimates[9,10] suggest that this mechanism alone would require substantially larger electric fields than are actually used by the experiments. This motivated Tsori *et al.*[9] to propose an additional effect involving mobile ions. However, we should not rule out the simple possibility that the apparent inconsistency lies with the accuracy of the current theoretical estimations.

Here we examine the dielectric mechanism with a newly developed self-consistent-field theory (SCFT) algorithm[11] in order to provide the most reliable quantitative predictions possible. As with the previous calculations,[8–10] this new approach implements the mean-field approximation, and treats the polymers as ideal linear dielectric materials. Beyond that, however, there are no further approximations, and the precision of our calculation is sufficiently stringent to render the numerical inaccuracies irrelevant. Furthermore, we investigate the detailed shape of the free-energy surface and, in particular, the size of the energy barrier along the kinetic pathway between spheres and perpendicular cylinders, as this is undoubtedly the main obstacle to any transition. Our study is performed on monolayer films, although it could, in principle, be extended to thicker films like those in the experiments of Ref. 8. Both systems will involve similar transformations with similar sized energy barriers, but multilayer films will possess a complicated network of potential pathways. This is because the spheres are staggered from layer to layer, implying a high degree of degeneracy in the way they fuse together to form cylinders. This degeneracy is libel to result in a final morphology with relatively poor order, although there may be ways of restoring order by, for example, cycling the field.[8] In any case, the complication is certainly avoided by using monolayer films. There will inevitably be practical challenges to working with such thin films, but presumably experiments are feasible. In addition to the potential applications, the relative simplicity of a monolayer film will make it an ideal model system for studying the underlying physics, and this is our main reason for choosing it.

II. THEORY

Here we present the SCFT for a melt of n AB diblock-copolymer molecules confined between two conducting plates charged to a potential difference of $V_0=E_0D_\parallel$ (see Fig. 1).[11] Our calculation assumes the melt is monodisperse with each diblock copolymer composed of N *coarse-grained* segments of which a fraction f forms the A block. The A and B segments are treated as incompressible with a common segment volume of ρ_0^{-1}, such that the total volume of the film is $\mathcal{V}=nN/\rho_0$. To limit the size of the parameter space, we restrict our attention to conformationally symmetric molecules where the A and B segments have the same statistical length (i.e., $a_A=a_B\equiv a$), although the extension to asymmetric lengths (i.e., $a_A\neq a_B$) is trivial.[12] The interaction between A and B segments is controlled by the usual Flory-Huggins χ parameter, and the electric-field effects are calculated assuming that the A and B components behave as linear isotropic materials with dielectric constants of κ_A and κ_B, respectively. The two surfaces at $z=0$ and $z=D_\parallel$ are treated with reflecting boundary conditions.[13,14] Again in the interest of a manageable parameter space, we assume that the surfaces have been modified to remove any preference for either block,[5] although it is straightforward to include a surface affinity if so desired.[15]

To investigate the transition from spheres to cylinders, we will examine the Landau-Ginzburg free-energy functional $F[\Phi]$ which provides the free energy for a specified composition profile $\Phi(\mathbf{r})$. (The usual equilibrium free energy of the film can be approximated by the global minimum of $F[\Phi]$.) In the spirit of mean-field theory, SCFT represents the net interaction experienced by A and B segments with two static fields,

$$w_A(\mathbf{r}) \equiv u(\mathbf{r}) + w(\mathbf{r}), \tag{1}$$

$$w_B(\mathbf{r}) \equiv u(\mathbf{r}) - w(\mathbf{r}), \tag{2}$$

respectively. Following standard techniques,[13] it is a straightforward matter to calculate the partition function $\mathcal{Q}$ of a single molecule and the dimensionless A and B segment concentrations $\phi_A(\mathbf{r})$ and $\phi_B(\mathbf{r})$, respectively. The fields $u(\mathbf{r})$ and $w(\mathbf{r})$ are then adjusted so as to satisfy the incompressibility assumption and the specified composition profile,

$$\phi_A(\mathbf{r}) + \phi_B(\mathbf{r}) = 1, \tag{3}$$

$$\phi_A(\mathbf{r}) - \phi_B(\mathbf{r}) = \Phi(\mathbf{r}), \tag{4}$$

respectively. Once that is done, the free energy is evaluated by

$$\frac{F[\Phi]}{nk_BT} = -\ln \mathcal{Q} - \frac{1}{\mathcal{V}}\int\left[\frac{\chi N}{4}\Phi^2(\mathbf{r}) + w(\mathbf{r})\Phi(\mathbf{r}) + u(\mathbf{r})\right]d\mathbf{r} - \mathcal{E}. \tag{5}$$

The logarithmic term provides the free energy of a single molecule in the field, while the integral accounts for the A-B interaction energy and simultaneously removes the fictitious field energy.

The last term in Eq. (5) represents the electrostatic energy stored in the film, $\mathcal{E}nk_BT=\frac{1}{2}V_0Q$, where $\pm Q$ is the charge on the plates. It may seem strange that this energy is subtracted from $F[\Phi]$ rather than added, but the argument for doing so is fairly simple. When the morphology varies, there will be a flow of charge, dQ, to the conductor in order to maintain a constant V_0, and this will cause the electrostatic energy to change by $\frac{1}{2}V_0dQ$. However, we must not forget that the energy of the power supply changes by $-V_0dQ$. Thus the net energy change is $-\frac{1}{2}V_0dQ$, which is exactly what we get if we omit the power supply and simply reverse the sign of $\mathcal{E}nk_BT$.[16]

Since it is difficult to evaluate Q, we express the electrostatic energy by the well-known expression[16]

$$\mathcal{E}nk_BT = \frac{\epsilon_0}{2}\int \kappa(\mathbf{r})|\mathbf{E}(\mathbf{r})|^2 d\mathbf{r}. \tag{6}$$

This way the calculation of $\mathcal{E}$ only requires the electric field $\mathbf{E}(\mathbf{r})$ between the plates, which obeys the Maxwell equations,

$$\nabla\cdot[\kappa(\mathbf{r})\mathbf{E}(\mathbf{r})] = 0, \tag{7}$$

$$\nabla\times\mathbf{E}(\mathbf{r}) = 0. \tag{8}$$

Here we have assumed that the polymer behaves as a linear dielectric material with

$$\kappa(\mathbf{r}) = \kappa_A\phi_A(\mathbf{r}) + \kappa_B\phi_B(\mathbf{r}) \tag{9}$$

$$= \frac{\kappa_A - \kappa_B}{2}\Phi(\mathbf{r}) + \frac{\kappa_A + \kappa_B}{2}. \tag{10}$$

Solving the Maxwell equations (7) and (8) is simplified by expressing the electric field as

$$\mathbf{E}(\mathbf{r}) = -E_0\nabla v(\mathbf{r}), \tag{11}$$

where $v(\mathbf{r})$ is the electric potential scaled with respect to the strength of the applied field, $E_0 \equiv V_0/D_\parallel$. This automatically enforces Eq. (8) and transforms Eq. (7) into

$$\nabla\cdot[\kappa(\mathbf{r})\nabla v(\mathbf{r})] = 0, \tag{12}$$

from which we only have to determine the scalar function $v(\mathbf{r})$. Once the potential is known, the electric-field energy can be evaluated by Eq. (6), but to make the calculation more tractable, we use the simpler expression

$$\mathcal{E}nk_BT = -\frac{\epsilon_0 E_0^2}{2}\int \kappa(\mathbf{r})\left[\frac{\partial}{\partial z}v(\mathbf{r})\right]d\mathbf{r}. \tag{13}$$

The equivalence of Eqs. (6) and (13) can be proven with the identity

$$\int \nabla(v+z)\cdot(\kappa\nabla v)d\mathbf{r} = \int (v+z)(\kappa\nabla v)\cdot d\mathbf{S} - \int (v+z)\nabla\cdot(\kappa\nabla v)d\mathbf{r}, \tag{14}$$

obtained using integration by parts. Noting that $v(\mathbf{r})+z=0$ at each plate and recalling Eq. (12), the surface and volume integrals on the right of the equality both vanish. This, in turn, implies that the volume integral on the left is also zero, from which the equivalence immediately follows.

To solve the SCFT equations, we follow the spectral technique developed in Ref. 13, where all spatially varying quantities $g(\mathbf{r})$ are expanded in a Fourier series,

$$g(\mathbf{r}) = \sum_i g_i f_i(\mathbf{r}). \tag{15}$$

Here, the technique is reproduced showing more of the details and using the generalized Fourier functions,

$$f_i(\mathbf{r}) = f_{\perp,i}(x,y)\cos(k_{z,i}z), \tag{16}$$

where the lateral symmetry of the morphology, in our case hexagonal (space group $p6mm$),[17] is built into $f_{\perp,i}(x,y)$. The z-dependent part of $f_i(\mathbf{r})$ enforces the reflecting boundary conditions at $z=0$ and $z=D_\parallel$ by setting $k_{z,i}\equiv\pi n_i/D_\parallel$ with n_i equal to an integer. As before,[11] the basis functions remain eigenfunctions of the Laplacian,

$$\nabla^2 f_i(\mathbf{r}) = -\left(\frac{\lambda_{\perp,i}}{D_\perp^2} + \frac{\pi^2 n_i^2}{D_\parallel^2}\right)f_i(\mathbf{r}), \tag{17}$$

and can be normalized to satisfy

$$\frac{1}{\mathcal{V}}\int f_i(\mathbf{r})f_j(\mathbf{r})d\mathbf{r} = \delta_{ij}. \tag{18}$$

The basis functions are ordered, $i=0,1,2,\ldots$, according to the magnitude of their eigenvalues, starting from $f_0(\mathbf{r})=1$ for which the eigenvalue to the Laplacian is zero. To perform actual calculations, the expansion has to be truncated, but we are careful to retain a sufficient number of functions so that the resulting numerical inaccuracy is irrelevant on the scale of our plots.

Since the electric potential obeys different boundary conditions (i.e., $v=0$ at $z=0$ and $v=-D_\parallel$ at $z=D_\parallel$), we expand it as

$$v(\mathbf{r}) = -z + \sum_i v_i\bar{f}_i(\mathbf{r}), \tag{19}$$

in terms of the complimentary basis functions,

$$\bar{f}_i(\mathbf{r}) = f_{\perp,i}(x,y)\sin(k_{z,i}z). \tag{20}$$

The sine function ensures that $\bar{f}_i(\mathbf{r})=0$ at the two conductors. Also notice that the partial derivative in Eq. (13) is now given by the simple expression

$$\frac{\partial}{\partial z}v(\mathbf{r}) = -1 + \sum_i k_{z,i}v_i f_i(\mathbf{r}). \tag{21}$$

In Fourier representation, the Landau-Ginzburg free-energy expression, Eq. (5), becomes

$$\frac{F[\Phi]}{nk_BT} = -\ln\mathcal{Q} - \sum_{i>0}\left(\frac{\chi N}{4}\Phi_i^2 + w_i\Phi_i\right) - \mathcal{E}, \tag{22}$$

where we have set $w_0=u_0=0$, since additive constants to the fields are of no consequence.[13] Furthermore, the Maxwell equation (12) reduces to

$$k_{z,i}\kappa_i = \sum_j H_{ij}v_j, \tag{23}$$

where $\mathbf{H}$ is a symmetric matrix. In the standard Fourier-series representation,[11] $H_{ij}=\mathbf{k}_i\cdot\mathbf{k}_j\kappa_k$, where k denotes the Fourier function corresponding to the wave vector $\mathbf{k}_k=\mathbf{k}_i-\mathbf{k}_j$. With our generalized functions, Eq. (16), the elements of $\mathbf{H}$ are more involved, but they still depend linearly on the dielectric coefficients κ_i. Once $\mathbf{H}$ has been evaluated, the coefficients of the electric potential are given by

$$v_i = \sum_j [H^{-1}]_{ij} k_{z,j} \kappa_j. \tag{24}$$

We also need to know how $v(\mathbf{r})$ changes with respect to $\kappa(\mathbf{r})$, which requires the derivatives

$$\frac{\partial v_i}{\partial \kappa_j} = \sum_k [H^{-1}]_{ik} G_{kj}, \tag{25}$$

where the components of $\mathbf{G}$ are given by

$$G_{ij} \equiv k_{z,i} \delta_{ij} - \sum_k \frac{\partial H_{ik}}{\partial \kappa_j} v_k. \tag{26}$$

In terms of the Fourier components, the electric-field energy, Eq. (13), is given by the simple expression

$$\mathcal{E} = \mathcal{E}_D \left(1 - \kappa_\Delta \sum_i k_{z,i} \Phi_i v_i \right), \tag{27}$$

where

$$\mathcal{E}_D = \frac{\epsilon_0 \bar{\kappa} E_0^2 \mathcal{V}}{2 n k_B T} \tag{28}$$

is the electrostatic energy for a disordered film and

$$\kappa_\Delta \equiv \frac{\kappa_A - \kappa_B}{2\bar{\kappa}}, \tag{29}$$

$$\bar{\kappa} \equiv f \kappa_A + (1-f) \kappa_B \tag{30}$$

specify the dielectric contrast and the average dielectric constant, respectively.

In order to characterize the detailed shape of the free-energy surface $F[\Phi]$, we need to know the change δF produced by a small variation in the composition profile $\delta\Phi(\mathbf{r})$. Following Ref. 18, the variation in free energy takes the form

$$\frac{\delta F}{n k_B T} = \sum_i \Omega_i \delta\Phi_i + \frac{1}{2} \sum_{ij} [\mathbf{C}_{\mathrm{RPA}}^{-1}]_{ij} \delta\Phi_i \delta\Phi_j + O(\delta\Phi^3). \tag{31}$$

The coefficients for the first-order terms are

$$\Omega_i = -w_i - \frac{\chi N}{2} \Phi_i - \frac{\partial \mathcal{E}}{\partial \Phi_i}, \tag{32}$$

where the derivatives of $\mathcal{E}$ are given by

$$\frac{\partial \mathcal{E}}{\partial \Phi_i} = -\mathcal{E}_D \kappa_\Delta \left(k_{z,i} v_i + \sum_j v_j G_{ji} \right). \tag{33}$$

Stable and metastable morphologies correspond to local minima in $F[\Phi]$, and thus are located by adjusting the fields so that $\Omega_i = 0$ for all $i > 0$, which are the usual self-consistent conditions that give SCFT its name. The coefficients for the second-order terms are

$$[\mathbf{C}_{\mathrm{RPA}}^{-1}]_{ij} = [\tilde{\mathbf{C}}^{-1}]_{ij} - \frac{\chi N}{2} \delta_{ij} - \frac{\partial^2 \mathcal{E}}{\partial \Phi_i \partial \Phi_j}. \tag{34}$$

The matrix $\tilde{\mathbf{C}}^{-1}$ accounts for variations in $-\ln \mathcal{Q}$ and is calculated by the method outlined in Refs. 18 and 19. The expression for the second-order derivatives of $\mathcal{E}$ is somewhat messy, and so we just evaluate them by numerical differentiation of Eq. (33). Once $\mathbf{C}_{\mathrm{RPA}}^{-1}$ is evaluated, its eigenvalues λ_α indicate the stability of the phase. The morphology is stable or metastable only if all the eigenvalues are positive.

The aim of this paper is to explore a representative *kinetic* pathway along the free-energy landscape $F[\Phi]$, starting from the minimum for spheres (S), traveling up to a saddle point from which the energy decreases towards the local minimum for cylinders (C). We actually start by locating the saddle point at the top of the path, which like the local minima is obtained by adjusting Φ_i so that $\Omega_i = 0$, for $i = 1, 2, 3, \ldots$. Unlike the local minima for S and C, the saddle point is unstable and thus $\mathbf{C}_{\mathrm{RPA}}^{-1}$ has a negative eigenvalue with the associate eigenvector defining the two directions in which $F[\Phi]$ decreases. We then follow these directions along the paths of steepest descent down the free-energy surface to the local minima for C and S. The surface is traversed in small steps of $\delta s = 0.01$, defined by the Euclidean metric,

$$\delta s^2 = \frac{1}{\mathcal{V}} \int \delta\Phi^2(\mathbf{r}) d\mathbf{r} = \sum_{i>0} \delta\Phi_i^2,$$

so that we can represent the free-energy surface by the expansion in Eq. (31). After each step, Ω and $\mathbf{C}_{\mathrm{RPA}}^{-1}$ are updated, and the process continues until a local free-energy minimum is reached where $\Omega_i = 0$. We arbitrarily set $s = 0$ at the top of the energy barrier, and define decreasing and increasing s as the directions toward S and C, respectively. It must be stressed that this construction only provides a representative pathway among many possible variations. However, the saddle point does correspond to the absolute minimum energy required for the system to complete the transition from S to C, and thus it does define a unique energy barrier.

As we traverse the kinetic pathway, there is an issue of whether or not to adjust the lateral periodicity $D_\perp$ to minimize $F[\Phi]$. In reality, it makes little difference to the calculation, because the preferred periodicities of S and C are reasonably well matched. Nevertheless, we choose to fix $D_\perp$ at the preferred value for the S morphology at zero electric field, because this is the state in which the film is initially annealed. We work on the assumption that the application of the electric field and the subsequent transformation to C will occur too rapidly for $D_\perp$ to respond. The justification is that any change in the periodicity requires a macroscopic transport of material, which is a relatively slow process. For example, even a tiny increase in $D_\perp$ requires each unit cell to acquire more material, which must come from its neighboring cells. The problem is that its neighbors are also in need of extra material. Some domains will ultimately have to be destroyed and their molecules distributed among the remaining ones. A decrease in $D_\perp$ creates the opposite problem, where new domains have to be nucleated.

III. RESULTS

We now examine the C to S transition in a thin film of diblock copolymer subjected to an applied electric field as illustrated in Fig. 1. Our parameter space has been greatly reduced by assuming that the diblock copolymers are confor-

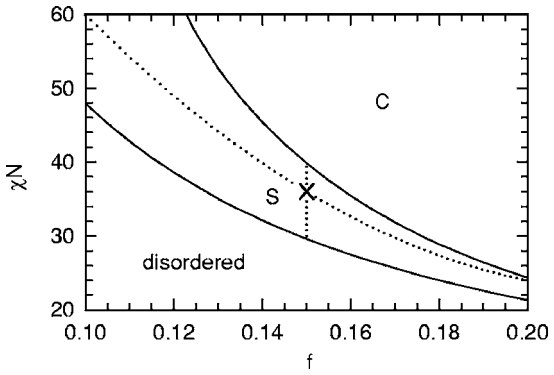

FIG. 2. Region S denotes the conditions under which a monolayer of hexagonally packed spheres has a lower free energy than either disordered or cylindrically ordered films, in the case of no external electric field. Most of our calculations focus on the point $\chi N=36$ and $f=0.15$ denoted by the cross, but we also investigate the effects from changes in segregation and composition along the two dotted paths.

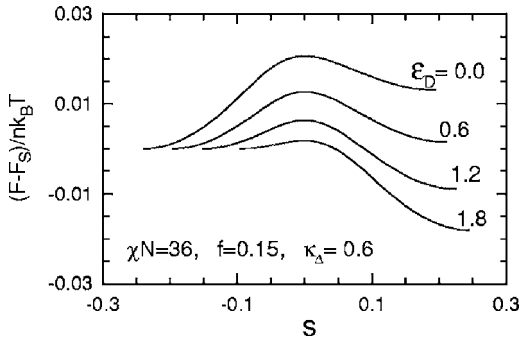

FIG. 4. Free energy F along the kinetic pathway from the minimum corresponding to a monolayer of spheres ($s<0$) up to the top of the energy barrier ($s=0$), and down to the minimum corresponding to perpendicular cylinders ($s>0$), plotted for external electric fields of various strengths $\mathcal{E}_D$. All four paths are calculated for block-copolymer films of segregation $\chi N=36$ and composition $f=0.15$, with a dielectric contrast of $\kappa_\Delta=0.6$.

mationally symmetric and that the parallel plates have been coated so as to remove any affinity for either component, but still the number of parameters remains rather large. Although confined films can be prepared with any thickness,[20] we will fix $D_\parallel$ by assuming that the spherical monolayer is in an unfrustrated state, where the film topography does not develop terraces upon removal of the top plate.[21] These special thicknesses are calculated using a free-energy construction described in Ref. 15, but we will use the simple fact that an unfrustrated film approximately corresponds to a minimum in F with respect to $D_\parallel$. In any case, we have confirmed that mild variations in $D_\parallel$ have no significant effect on our results.

Even with our assumptions, there are four remaining parameters: the segregation of the unlike segments χN, the diblock composition f, the dielectric contrast κ_Δ, and the electric-field strength $\mathcal{E}_D$. Before the application of the electric field, the film will have to be annealed for a prolonged period in order to create good hexagonal order among the spherical domains. Thus, the block-copolymer parameters must be selected within the spherical (S) region of Fig. 2. If χN is too small then the morphology will disorder, and if it is too large the film will develop cylindrical (C) domains with presumably a horizontal orientation.

Our study begins with a detailed examination of films prepared and annealed at $\chi N=36$ and $f=0.15$, as indicated by the cross in Fig. 2. In the absence of the field, the free energy F_S of the S morphology is minimized for a film thick of $D_\parallel/aN^{1/2}=1.406$ and a nearest-neighbor separation between spheres of $D_\perp/aN^{1/2}=1.532$. Despite the hexagonal shape of the unit cell, the minority domain is nearly a perfect sphere as illustrated by the cross section shown in Fig. 3. However, as soon as an electric field is applied, the domain transforms into an ellipsoidal shape with its long axis oriented in the direction of the field.

Figure 4 illustrates the effect of an electric field on the kinetic pathway from the S to the C morphology, assuming a dielectric contrast of $\kappa_\Delta=0.6$. For field strengths of $\mathcal{E}_D>0.682$, the free energy of perpendicular cylinders F_C drops below that of the spheres, F_S, and the transition to C can, in principle, proceed. However, the high energy of the saddle point, F_B, will tend to prevent the transition, and consequently stronger fields are generally required. By $\mathcal{E}_D\approx 1.8$, the energy barrier, F_B-F_S, is virtually gone, and the transition can presumably be initiated by thermal fluctuations. Just how small the energy barrier needs to be is an issue that we will discuss in the next section.

The transformation of the minority domain is illustrated in Fig. 5 as the system evolves along the kinetic pathway from S to C under an applied electric-field strength of $\mathcal{E}_D=1.8$. The second image at $s=0$ corresponds to the top of the energy barrier, which may take the system numerous attempts in order to reach. However, once the system makes it to this point, the rest of the transformation is downhill and will occur rapidly. After the C phase has formed, it should, in principle, adjust to its equilibrium spacing of $D_\perp/aN^{1/2}$

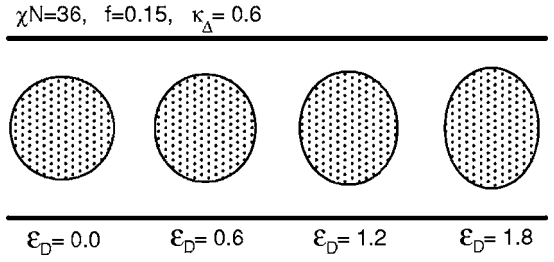

FIG. 3. Deformation of a spherical nanodomain [defined by $\Phi(\mathbf{r})>0$] as the electric-field strength $\mathcal{E}_D$ is increased. Note that the hexagonal packing of the domains has little effect on the rotational symmetry about their vertical axes. Therefore, we only show a single cut through the sphere, where the horizontal axis points in the direction of a nearest neighbor.

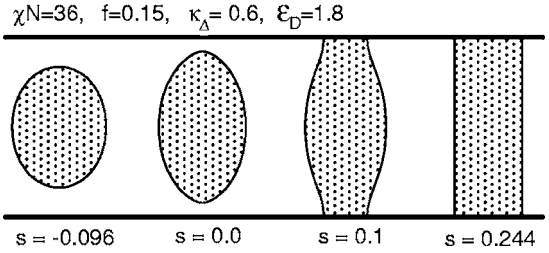

FIG. 5. Evolution of the minority domain along the kinetic pathway shown in Fig. 4 for the field strength of $\mathcal{E}_D=1.8$. The positions $s=-0.0959$, $s=0.0$, and $s=0.2438$ along the pathway correspond to the free-energy minimum of the S phase, the top of the energy barrier, and the minimum of the C phase, for which the free energies are denoted by F_S, F_B, and F_C, respectively.

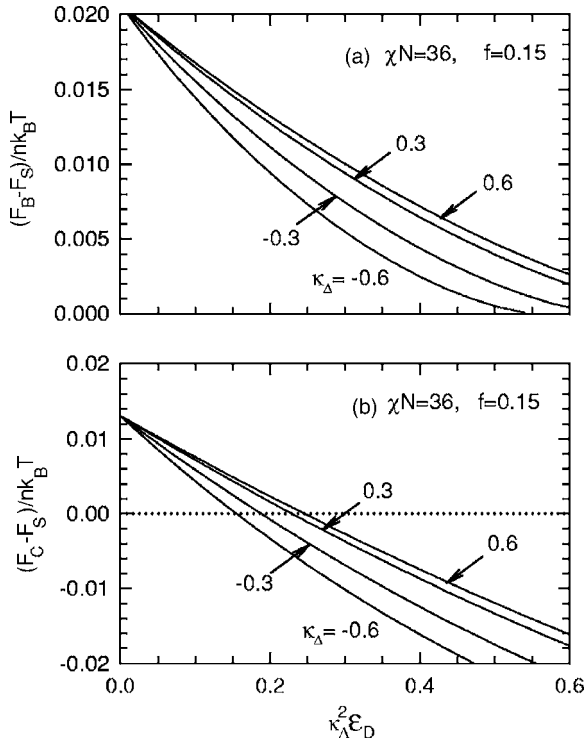

FIG. 6. (a) Energy barrier, F_B-F_S, preventing the transformation from spheres to cylinders and (b) relative stability of the cylinders, F_C-F_S, plotted as a function of increasing field strength $\mathcal{E}_D$ for several values of the dielectric contrast κ_Δ. To combine results for different κ_Δ, the horizontal axes have been scaled by κ_Δ^2.

$=1.575$. This would reduce the total number of domains by $\sim 5\%$, and would undoubtedly have a disruptive effect on the hexagonal order. However, the available reduction in free energy is $0.000\,93 k_B T$ per molecule, which corresponds to only about twice the linewidth used in Fig. 4. Considering the tiny energy gain, the adjustment in $D_\perp$ is certain to be extremely slow, likely exceeding the time scale of any reasonable experiment.[22]

Figure 6 examines the reduction in the free-energy barrier, F_B-F_S, and the increased stability of the cylinders, F_C-F_S, as a function of field strength $\mathcal{E}_D$ for several different dielectric contrasts κ_Δ. The results are plotted in accord with a standard approximation for the electrostatic energy,[8,9,16] where the net effect is determined solely by $\kappa_\Delta^2\mathcal{E}_D$. If the effect was indeed entirely dependent upon this product, there would be a considerable advantage of synthesizing the matrix block from the low-dielectric contrast segments, because this would result in a smaller value of $\bar{\kappa}$, which, in turn, produces a larger $\kappa_\Delta^2\mathcal{E}_D$. However, our more refined results in Fig. 6 show that $\kappa_\Delta^2\mathcal{E}_D$ does not need to be as large to create the same effect when the dielectric contrast is negative. Even still, it remains advantageous to choose the low-dielectric contrast material for the matrix, but not nearly as much as suggested by the approximate calculations.[8,9,16]

Now we investigate films prepared at different levels of segregation χN, but with the same composition, $f=0.15$, which corresponds to the vertical dotted line in Fig. 2. Figure 7(a) shows that there is a slight reduction in the energy barrier, F_B-F_S, as the segregation is increased, but it is not particularly significant. Much more significant is the effect

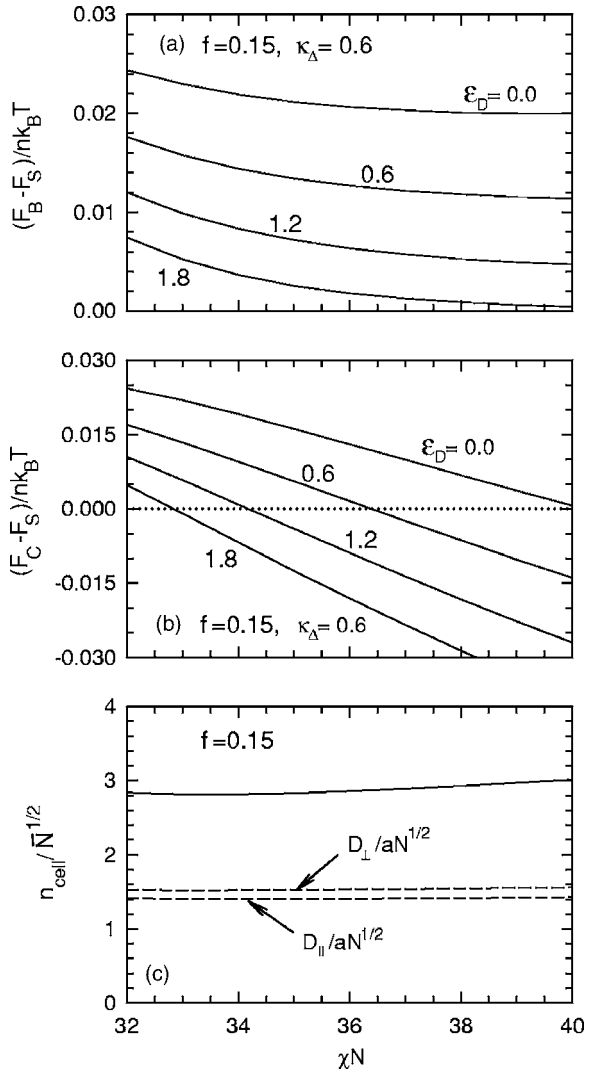

FIG. 7. (a) Energy barrier, F_B-F_S, preventing the transformation from spheres to cylinders and (b) relative stability of the cylinders, F_C-F_S, plotted as a function of segregation χN for several different field strengths $\mathcal{E}_D$. The diblock composition and dielectric contrast are fixed at $f=0.15$ and $\kappa_\Delta=0.6$, respectively. (c) Number of molecules n_{cell} per nanodomain (solid curve) along with the dimensions of its unit cell (dashed curves).

χN has on the relative stability of the perpendicular cylinders. The reduction in F_C-F_S is useful since it has to be negative for the transition to occur, but it is also important that F_C-F_S be sufficiently positive in the zero-field limit for the formation of the initial spherical morphology. Thus, it is best that the film is prepared and annealed at a segregation somewhat below the S/C boundary in Fig. 2.

Figure 8 provides analogous plots to those in Fig. 7, but this time showing the effect of varying the composition f. So as to stay within the S region, the segregation is adjusted according to $\chi N=24(100f^2-45f-6)$ as we sweep across the f range; the path is denoted in Fig. 2 by a dotted curve. The general conclusion from Fig. 8 is that the energy differences among F_S, F_B, and F_C are reduced as the diblock becomes more symmetric. Indeed, the $\mathcal{E}_D=1.2$ and 1.8 curves in Fig. 8(a) reach zero, beyond which the energy barrier is completely abolished. When this happens, the local free-energy minimum for the S phase actually vanishes, which is why the corresponding curves in Fig. 8(b) suddenly end. The impli-

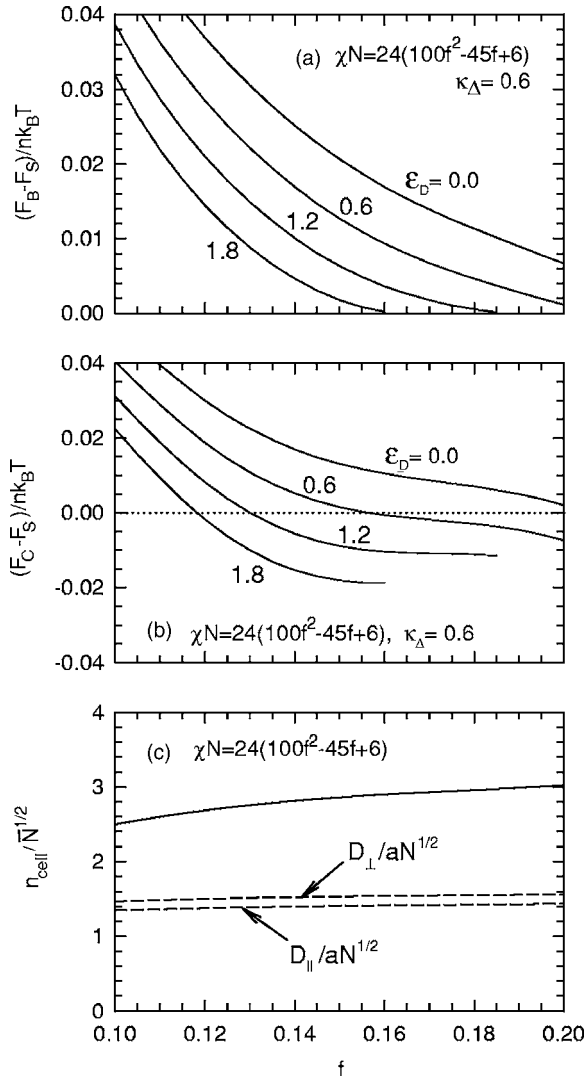

FIG. 8. Analogous plots to those in Fig. 7, but showing the effect of changing the diblock-copolymer composition f. In order that the monolayer of spheres remains stable under zero electric field, the segregation is adjusted according to $\chi N=24(100f^2-45f+6)$, which is denoted by a dotted curve in Fig. 2.

cation is that the diblock composition should be chosen as symmetric as possible, but of course there is a limit to how far one can go. If the free-energy minima become too shallow, then thermal (Brazovskii) fluctuations will prevent the formation of ordered morphologies.[23]

IV. DISCUSSION

We have examined the ability of an applied electric field to convert a monolayer of hexagonally packed spheres (S) into perpendicular cylinders (C), using the state-of-the-art theory developed in Ref. 11. The general trends elucidated by our study provide valuable guidance on how to optimize the system parameters in order to avoid dielectric breakdown. To summarize, a high dielectric contrast, $|\kappa_\Delta|$, is of prime importance in reducing the necessary field E_0. It is also best to place the low-dielectric contrast component in the matrix so that $\bar{\kappa}$ is small. This follows from the fact that the electric-field effect is approximately determined by the product $\kappa_\Delta^2 \mathcal{E}_D$, which is inversely proportional to $\bar{\kappa}$ for fixed $|\kappa_A-\kappa_B|$. The molecular weight of the diblock copolymer should be chosen such that χN is close to the S/C boundary in Fig. 2, but still sufficiently inside the S region so that the initial annealing produces a well-ordered array of spheres. Finally, the diblock composition f should be chosen as symmetric as possible in order to minimize the energy barrier.

Ideally, a sufficient electric field should be applied so as to eliminate the energy barrier altogether, allowing the transition to proceed unobstructed. However, even if dielectric breakdown prevents the use of such field strengths, the system might still overcome the energy barrier via thermal fluctuations. To estimate the size of barrier that can be circumvented in a realistic time scale, we need to know the approximate number of molecules involved. We make the reasonable assumption that the spheres transform into cylinders one at a time, and thus the number of molecules involved are those of a single nanodomain. Since the volume of the unit cell is $\sqrt{3}D_\parallel D_\perp^2/2$ and the volume of each molecule is N/ρ_0, where ρ_0 is the volume density of segments, the number of molecules is

$$n_{\text{cell}} = \frac{\sqrt{3}}{2}\frac{D_\parallel D_\perp^2}{a^3 N^{3/2}}\bar{N}^{1/2}, \tag{35}$$

where $\bar{N}\equiv\rho_0^2 a^6 N$ is the invariant polymerization index, for which typical values range from $\bar{N}\sim 10^3$ to 10^5.[24] Based on Figs. 7(c) and 8(c), we can expect between $n_{\text{cell}}\sim 10^2$ and 10^3 molecules per domain. Thus the typical energies barriers of $(F_B-F_S)/nk_BT\sim 0.01$ predicted by our study are within the regime where fluctuations can be effective, provided that f is not too small and $\bar{N}$ is not too large.

There have yet to be electric-field experiments on spherical monolayers, but Xu *et al.*[8] have examined thicker films containing approximately ten layers of polymethylmethacrylate (PMMA) spheres in a polystyrene (PS) matrix. Consistent with our assumptions, their conducting plates were coated with PMMA-PS random copolymer brushes of appropriate composition to negate any surface affinity, and the conformational asymmetry, $a_{\text{PMMA}}/a_{\text{PS}}=1.07$, is more or less negligible, based on tabulated values in Ref. 25 for 140 °C. Xu *et al.* found that an electric field of $E_0\approx 40$ V/μm applied for 20 h at 170 °C was able to fuse spherical domains together to form cylindrical domains oriented in the field direction. Although the experiment was for a multilayer film, the free energies involved in transforming spheres into cylinders are similarly enough to make a reasonable quantitative comparison to our calculations; this follows from the fact that the surfaces behave as reflecting boundaries.[13,14] The PMMA-PS diblock copolymers in the experiment were quoted to have a PMMA volume fraction of $f=0.1$. Using the data from Ref. 25, we estimate that $\bar{N}=4300$, $aN^{1/2}=26$ nm, and $n_{\text{cell}}=160$. Based on the dielectric constants of PMMA and PS,[8] $\kappa_\Delta=0.61$ and $\bar{\kappa}=2.9$ from which the effective field strength works out to be $\mathcal{E}_D=0.84$. Applying our calculation at $\chi N=60$, we obtain an energy barrier of $6.7k_BT$. Although the energy barrier in the experimental system must have been several k_BT given the long conversion time of about 20 h, our prediction of $6.7k_BT$ seems a bit too high. The more serious concern is that $\mathcal{E}_D=0.84$ turns out to be insufficient to

stabilize C relative to S. Assuming higher values of χN improves the situation slightly, but not nearly enough to be consistent with the experimental value of $\mathcal{E}_D$.

Tsori *et al.*[9] have suggested that the mechanism is not entirely due to a simple coupling between the electric field and the dielectric contrast, but that it also has to do with the presence of Li^+ ions. We suggest that there are other plausible explanations. For example, the discrepancy could be attributed to inaccuracies in the theory combined with experimental uncertainties. Although we have performed the most accurate calculation to date, it still contains some significant approximations. The mean-field treatment is likely accurate, because the morphology is evidently well segregated (i.e., the PS and PMMA domains are relatively pure), but the Gaussian chain model[13] may not be so accurate for the relatively short PMMA blocks. Also, nonlinear polarization effects are likely to be significant for such strong electric fields. On the experimental side, the most obvious source of uncertainty is the estimate for f; an error of +0.04 would itself be enough to account the discrepancy between experiment and theory. Even trace amounts of impurities in the experimental film (i.e., residual solvent and random copolymers that have detached from the plates) could have a contributing factor. Considering all the possible explanations, the difference between theory and experiment is not all that alarming.

In addition to being relatively accurate, our SCFT-based treatment is also sufficiently versatile to account for the extra effects described above. There are already multicomponent versions of SCFT (Ref. 26) to cope with additional species, such as residual solvent molecules. If some of the species are charged, such as Li^+ ions, this just requires the Maxwell equation (7) to be generalized to $\nabla\cdot(\kappa\mathbf{E})=\rho_f/\epsilon_0$, where $\rho_f(\mathbf{r})$ is the combined density of all the *free* charges. Our treatment could also explicitly include the random copolymer brushes used by Xu *et al.* to neutralize the surface affinities.[27] In fact, none of these extensions would be all that computationally demanding. The only real challenge would be to cope with all the extra parameters that it would entail.

Several previous theoretical studies have examined the electric-field-induced sphere-to-cylinder transformation, although for bulk and thick-film systems. However, all but one involved additional approximations beyond the mean-field and linear-dielectric approximations used in our study. The first calculation by Tsori *et al.*[9] was supplemented by a weak-segregation approximation that is relatively inaccurate for asymmetric molecules (i.e., $f\approx 0.15$). Even next to the order-disorder transition (ODT), the segregation is far from weak, which is why such theories[28] are unable to account for the close-packed arrangement of spheres in the bulk phase diagram.[29] In addition, Tsori *et al.* treated the electrostatic energy using an approximation appropriate to weak electric fields.[16] Shortly after, Xu *et al.*[8] presented an improved SCFT-based calculation, but they also invoked a similar approximation for the electrostatic energy. Furthermore, they perform their calculation in real space with a relatively coarse mesh, and so their results are presumably affected by a significant degree of numerical inaccuracy.

The one study on the relative stability of the bulk S and C phases that did perform the mean-field and electric-field calculations exactly is that of Lin *et al.*[10] However, the equivalence of their approach to that[11] of ours is not immediately obvious because of the way they derive their field equations. They start with the usual requirement, which for the A segments is given by

$$\frac{1}{nk_BT}\frac{\mathcal{D}F}{\mathcal{D}\phi_A(\mathbf{r})}=\frac{1}{\mathcal{V}}[\chi N\phi_A(\mathbf{r})-w_A(\mathbf{r})+\xi(\mathbf{r})]-\frac{\mathcal{D}\mathcal{E}}{\mathcal{D}\phi_A(\mathbf{r})}=0. \tag{36}$$

The questionable step is when Lin *et al.* evaluate the functional derivative of $\mathcal{E}$ as

$$\frac{\mathcal{D}\mathcal{E}}{\mathcal{D}\phi_A(\mathbf{r})}=\frac{\epsilon_0\kappa_A}{2nk_BT}|\mathbf{E}(\mathbf{r})|^2, \tag{37}$$

by holding $\mathbf{E}(\mathbf{r})$ fixed and only allowing $\kappa(\mathbf{r})$ to vary. Normally, both quantities must vary together in order to comply with the Maxwell equation (7). The missing justification in Ref. 10 is that

$$\frac{\mathcal{D}\mathcal{E}}{\mathcal{D}v(\mathbf{r})}=-\frac{\epsilon_0E_0^2}{nk_BT}\nabla\cdot[\kappa(\mathbf{r})\nabla v(\mathbf{r})]=0, \tag{38}$$

for fixed $\kappa(\mathbf{r})$, but this is only true if one uses Eq. (6) with the electric field substituted by $\mathbf{E}(\mathbf{r})=-E_0\nabla v(\mathbf{r})$. If one instead uses Eq. (13) for the electrostatic energy, then

$$\frac{\mathcal{D}\mathcal{E}}{\mathcal{D}v(\mathbf{r})}=\frac{\epsilon_0E_0^2}{2nk_BT}\frac{\partial}{\partial z}\kappa(\mathbf{r})\neq 0, \tag{39}$$

and the justification for holding $\mathbf{E}(\mathbf{r})$ fixed is no longer valid. Consequently, our self-consistent-field condition (i.e., $\Omega_i=0$) would have been wrong had we treated v_i in Eq. (27) as a constant when evaluating Eq. (33). This demonstrates the importance of understanding the underlying reason why $\mathbf{E}(\mathbf{r})$ could be held fixed in the derivation of Lin *et al.*

V. CONCLUSIONS

We have investigated the free-energy landscape $F[\Phi]$ of a diblock-copolymer thin film as a function of its composition profile $\Phi(\mathbf{r})$. The study focused on the effect an applied electric field, $E_0\equiv V_0/D_\parallel$, has on the kinetic pathway from the local free-energy minimum for a monolayer of spherical (S) domains to that of perpendicular cylindrical (C) domains (see Fig. 1). The application of the field brings about the global stability of the (C) morphology (i.e., $F_C<F_S$), while at the same time diminishing the energy barrier (i.e., $F_B\rightarrow F_S$) separating the two minima. The optimum conditions for inducing the $S\rightarrow C$ transition, while avoiding dielectric breakdown, require a large dielectric contrast with the matrix composed of the low-dielecctric contrast material. Furthermore, the segregation χN should be chosen such that the film is in the S region of Fig. 2 close to but not too close to the C/S boundary. Finally, the diblock composition f should be as symmetric as possible, short of entering the weak-segregation regime where the ordered morphologies are destroyed by Brazovskii fluctuations.

Our calculations have been performed using a spectral-based technique developed in Ref. 11, where the self-consistent-field theory (SCFT) for block copolymers[13] was supplemented with an exact treatment for linear dielectric materials. Here we have improved the efficiency of our original algorithm by incorporating the symmetry of the morphology into the basis functions. This method of investigating the free-energy landscape uses the most accurate treatment of electric-field effects to date, and offers a unique opportunity for quantitative comparisons with experiment. It also possesses the versatility needed to investigate added effects due to, for example, residual solvent, mobile ions, and brush-coated plates. With such abilities, the theory is well posed to make significant headways in our understanding of electric-field effects in block-copolymer thin films.

ACKNOWLEDGMENT

We are grateful to Glenn Fredrickson for informing us that the functional derivation in Eq. (38) is zero, thus providing justification for the field equations used in Ref. 10.

[1] I. W. Hamley, Nanotechnology **14**, R39 (2003); R. A. Segalman, Mater. Sci. Eng., R. **48**, 191 (2005).
[2] S. G. Xiao, X. M. Yang, E. W. Edwards, Y. H. La, and P. F. Nealey, Nanotechnology **16**, S324 (2005); T. Thurn-Albrecht, J. Schotter, G. A. Kästle, N. Emley, T. Shibauchi, L. Krusin-Elbaum, K. Guarini, C. T. Black, M. T. Tuominen, and T. P. Russell, Science **290**, 2126 (2000).
[3] M. Park, C. Harrison, P. M. Chaikin, R. A. Register, and D. H. Adamson, Science **276**, 1401 (1997).
[4] J. Rzayev and M. A. Hillmyer, Macromolecules **38**, 3 (2005); M. A. Hillmyer, Adv. Polym. Sci. (in press).
[5] P. Mansky, Y. Lui, E. Huang, T. P. Russell, and C. Hawker, Science **275**, 1458 (1995); J. Genzer and E. J. Kramer, Phys. Rev. Lett. **78**, 4946 (1997).
[6] R. A. Segalman, A. Hexemer, and E. J. Krammer, Phys. Rev. Lett. **91**, 196101 (2003); Macromolecules **36**, 6831 (2003).
[7] T. L. Morkved, M. Lu, A. M. Urbas, E. E. Ehrichs, H. M. Jaeger, P. Mansky, and T. P. Russell, Science **273**, 931 (1996).
[8] T. Xu, A. V. Zvelindovsky, G. J. A. Sevink, O. Gang, B. Ocko, Y. Zhu, S. P. Gido, and T. P. Russell, Macromolecules **37**, 6984 (2004).
[9] Y. Tsori, F. Tournilhac, D. Andelman, and L. Leibler, Phys. Rev. Lett. **90**, 145504 (2003).
[10] C.-L. Lin, M. Schick, and D. Andelman, Macromolecules **38**, 5766 (2005).
[11] M. W. Matsen, Phys. Rev. Lett. **95**, 258302 (2005).
[12] M. W. Matsen and F. S. Bates, J. Polym. Sci., Part B: Polym. Phys. **35**, 945 (1997).
[13] M. W. Matsen, in *Soft Matter*, edited by G. Gompper and M. Schick (Wiley-VCH, Weinheim, 2006), Vol. I.
[14] A. Silberberg, J. Colloid Interface Sci. **90**, 86 (1982).
[15] M. W. Matsen, J. Chem. Phys. **106**, 7781 (1997).
[16] K. Amundson, E. Helfand, X. N. Quan, and S. D. Smith, Macromolecules **26**, 2698 (1993); K. Amundson, E. Helfand, X. N. Quan, S. D. Hudson, and S. D. Smith, *ibid.* **27**, 6559 (1994).
[17] *International Tables for X-ray Crystallography*, edited by N. F. M. Henry and K. Lonsdale (Kynoch, Birmingham, 1969).
[18] A.-C. Shi, J. Noolandi, and R. C. Desai, Macromolecules **29**, 6487 (1996).
[19] M. W. Matsen, Phys. Rev. Lett. **80**, 4470 (1998); J. Chem. Phys. **114**, 8165 (2001).
[20] P. Lambooy, T. P. Russell, G. J. Kellogg, A. M. Mayes, P. D. Gallagher, and S. K. Satija, Phys. Rev. Lett. **72**, 2899 (1994); N. Koneripalli, N. Singh, R. Levicky, F. S. Bates, P. D. Gallagher, and S. K. Satija, Macromolecules **28**, 2897 (1995).
[21] G. Coulon, T. P. Russell, V. R. Deline, and P. F. Green, Macromolecules **22**, 258 (1989); T. P. Russell, G. Coulon, V. R. Deline, and D. C. Miller, *ibid.* **22**, 4600 (1989).
[22] P. M. Lipic, F. S. Bates, and M. W. Matsen, J. Polym. Sci., Part B: Polym. Phys. **37**, 2229 (1999).
[23] G. H. Fredrickson and E. Helfand, J. Chem. Phys. **87**, 697 (1987).
[24] F. S. Bates, M. F. Schulz, A. K. Khandpur, S. Förster, J. H. Rosedale, K. Almdal, and K. Mortensen, Faraday Discuss. **98**, 7 (1994).
[25] L. J. Fetters, D. J. Lohse, D. Richter, T. A. Witten, and A. Zirkel, Macromolecules **27**, 4639 (1994).
[26] K. M. Hong and J. Noolandi, Macromolecules **14**, 727 (1981); M. W. Matsen, Phys. Rev. Lett. **74**, 4225 (1995).
[27] M. W. Matsen and J. M. Gardiner, J. Chem. Phys. **115**, 2794 (2001).
[28] L. Leibler, Macromolecules **13**, 1602 (1980).
[29] M. W. Matsen and F. S. Bates, Macromolecules **29**, 1091 (1996).